A New Control Strategy for Three-Phase Shunt Active Power Filters Based on FIR Prediction

Osman Kukrer, *Senior Member IEEE,* Hasan Komurcugil, *Senior Member IEEE,*
Ramon Guzman, and Luis Garcia de Vicuna

***Abstract*—A new discrete-time control strategy for three-phase three-wire shunt active power filters (APF) is presented, based on a mathematical model in the stationary reference frame. It involves a feedback-linearization-type approach to control the filter currents, whereby the voltage control loop is decoupled from the current control. The voltage control loop is for controlling the dc-side voltage of the PWM converter, and employs a proportional-integral (PI) controller to generate the reference amplitude for the compensated grid currents. An important feature of the proposed control strategy is the compensation of the one-sampling-period delay caused by microcontroller computation using a finite impulse response (FIR) predictor. This predictor is designed to accomplish one-step-ahead prediction of the control variable, which is the PWM converter's switching function space vector. Furthermore, the FIR predictor is optimized so that the low order harmonics in the control variable are predicted with minimal error. The proposed control strategy is analyzed to obtain the steady state filter current error and ranges for the PI controller gains for stability. Simulation and experimental results are presented to show the effectiveness of the proposed shunt APF.**

***Index Terms*—Shunt active power filter, predictive control, FIR predictor**

I. INTRODUCTION

DUE to the rapidly growing use of power-electronics devices in domestic, industrial and commercial equipment, the harmonic current distortion on the grid has increased considerably in recent years. It is well known that the distorted grid currents cause voltage drops on grid network impedances which may lead to unbalanced conditions. Distorted grid currents can also cause poor power factor, increase heating losses, and affect other loads connected at the point of common coupling (PCC). Therefore, the current harmonics injected into the grid should be kept below the specified limits [1].

Manuscript received February 10, 2020; revised May 18, 2020 and July 6, 2020; accepted July 19, 2020.

O. Kukrer is with the Electrical and Electronic Engineering Department, Eastern Mediterranean University, 99628 Famagusta, Mersin 10, Turkey. (e-mail: osman.kukrer@emu.edu.tr).

H. Komurcugil is with the Computer Engineering Department, Eastern Mediterranean University, 99628 Famagusta, Mersin 10, Turkey. (corresponding author: e-mail: hasan.komurcugil@emu.edu.tr).

R. Guzman is with the Department of Automatic Control, Technical University of Catalonia, 08800 Barcelona, Spain. (e-mail: ramon.guzman@upc.edu).

L. G. de Vicuna is with the Department of Electronic Engineering, Technical University of Catalonia, 08800 Barcelona, Spain. (e-mail: vicuna@upc.edu).

Although conventional passive filters can be employed for compensating the undesired harmonics, they have many drawbacks such as resonance, fixed compensation ability, and large size. In contrast, shunt active power filters (APFs) are widely used for compensating the undesired current harmonics [2]. When a shunt APF is connected to the PCC, it injects compensating currents having the same amplitude and opposite phase to those of the load current harmonics so as to obtain sinusoidal grid currents in phase with the grid voltages. In order to achieve this, the APF should be controlled by an appropriate control strategy which possesses several features such as fast dynamic response, good current tracking capability, robustness to parameter variations, low total harmonic distortion (THD) in the grid currents, and good dc bus voltage regulation. Generally, a control strategy consists of three parts, namely: 1) generation of the reference compensating current; 2) current-control of the voltage-source PWM converter; and 3) control of the dc bus voltage. Generation of the reference compensating current plays an important role that affects the filtering performance since any inaccurate phase and magnitude of reference compensating currents result in degradation in the compensation process. Various control strategies have been studied in the literature to achieve these requirements.

Synchronous reference frame (d-q transformation) [3], instantaneous reactive power theory (p-q transformation) [4], notch-filter-based theory [5], and Kalman-filter-based theory [6], [7] are the commonly used approaches for generating the reference compensating current. In [8], a new approach based on double reduced-order generalized integrators (DROGI) is proposed for extracting reference compensating current. Having generated the reference compensating current, a current-control strategy should be developed that forces the filter current to track its reference. Proportional-integral (PI) control strategy leads to steady-state errors and does not exhibit a satisfactory performance due to its control bandwidth limitation [3]. The linear quadratic regulator (LQR) strategy proposed in [9] exhibits satisfactory performance, but it involves too many gains which require fine tuning for a good performance. Other types of current control strategies proposed for shunt APFs include power balance theory [10], direct current space vector control [11], adaptive control [12], [13], advanced current control [14], one-cycle control [15], direct power control [16], virtual flux based control [17], and optimized compensation approach [18].

The development of switching devices and availability of powerful and cheaper digital signal processor (DSP) and field-

programmable-gate-array (FPGA) based systems has made possible the implementation of new digital control strategies such as the digital control [19], repetitive control [20]-[22], fuzzy control [23], [24], p-q theory based control [25], deadbeat control [26], and adaptive linear neural network based control [27]. The deadbeat control method offers fast dynamic response, but its performance is dependent on the system parameters. The repetitive control strategy copes with the periodic disturbances successfully, but it suffers from the poor performance to non-periodic disturbances.

The predictive control which is also suitable for DSP and FPGA implementation has the advantage that the future behavior of the controlled variables can be predicted by using the model of the APF system. The predicted variables are then utilized by the controller so as to obtain the desired action determined by the preset optimization criterion. The first predictive current control strategy applied to the control of shunt APF was proposed in [28]. Thereafter, its properties with the combination of artificial neural networks have been utilized in the generation of reference compensating currents [29]. One-sample-period-ahead based predictive control proposed in [30] has the ability to predict the controlled variables one and two sampling periods in advance. On the other hand, model predictive control (MPC) has emerged as an alternative to the classical predictive control methods aiming at minimizing a cost function [31], [32]. However, MPC requires excessive computations during small sampling period. The finite control set MPC (FCS-MPC) is formulated on the discrete nature of the converter and does not require an external modulator [33]-[35]. The effectiveness of FCS-MPC was investigated on the multilevel APFs such as single-phase neutral-point clamped (NPC) converter based AFP [33] and three-phase four-leg flying capacitor converter based APF [34]. In [35], a FCS-MPC is proposed for shunt APF. Unlike the existing control methods, the proposed control method employs a modulator for alleviating the current ripple and improving the performance of the APF. The authors in [36] proposed a least mean square (LMS) based adaptive linear element (Adaline) control strategy which needs one current sensor and one voltage sensor only.

In this paper, the continuous-time control approach presented in [37] is adopted in discrete-time. Also, an additional gain is included into the current control loop to damp the current faster. However, computation delay and uncertainties in the system parameters arise as the main problems during the discrete-time implementation. Therefore, the work presented here aims to address these issues. The proposed approach possesses the following features: (i) the current control loop is decoupled from the voltage loop by the applied feedback linearization, (ii) the computation delay is compensated by the optimized finite impulse response (FIR) predictor, (iii) the closed-loop poles are not sensitive to an uncertainty in the filter inductance. The optimized FIR allows the prediction of the low order harmonics in the control variable with minimal error. Also, unlike the existing predictive control strategies which are generally based on the filter model, the dependence of the controller on the filter inductance is minimized. In [38], moving average FIR filter is employed to remove the harmonics in the load current. In [39], FIR filter is used to estimate the reference grid current. However, the use of FIR filter in these studies does not target to resolve the compensation of the computation delay. The performance of the proposed APF is investigated through simulations and experimentally.

II. THE APF MODEL IN STATIONARY REFERENCE FRAME

Fig. 1 shows a three-phase shunt APF. The ac source supplies a three-phase nonlinear load which draws non-sinusoidal currents. The APF which is connected to the point of common coupling (PCC) is based on the boost PWM converter topology with six switching devices. These switching devices should be operated in such a way that the three-phase source currents are sinusoidal and in phase with the three-phase source voltages. The equation describing the operation of the APF in the stationary reference frame can be written in the vector form as follows

$$R_l \mathbf{i}_c + L\frac{d\mathbf{i}_c}{dt} = \mathbf{e} - \tfrac{1}{2}\mathbf{d}\,v_c \tag{1}$$

where $\mathbf{i}_c$ denotes filter current space vector, $\mathbf{e}$ denotes the source voltage space vector, $\mathbf{d}$ denotes the switching function space vector and R_l is the resistance of the coupling inductor. It is worth to note that the space vector of a three-phase quantity can be defined as

$$\mathbf{w} = \tfrac{2}{3}(w_a + \mathbf{a}\,w_b + \mathbf{a}^2 w_c) \quad , \quad \mathbf{a} = e^{j2\pi/3} \tag{2}$$

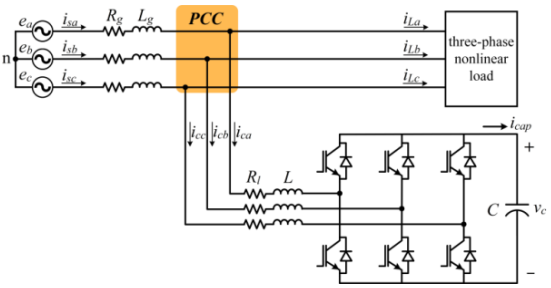

Fig. 1. Three-phase shunt APF.

The three-phase line-to-neutral source voltages can be defined as

$$e_a(t) = E_m\cos(\omega t)\,,\; e_b(t) = E_m\cos(\omega t - \tfrac{2\pi}{3})\,,\; e_c(t) = E_m\cos(\omega t + \tfrac{2\pi}{3}) \tag{3}$$

Using the definition in (2), the source voltage space vector can easily be obtained as

$$\mathbf{e} = E_m e^{j\omega t} \tag{4}$$

The capacitor current in terms of the filter current vector and switching function space vector can be written as [37]

$$i_{cap} = C\frac{dv_c}{dt} = \frac{3}{8}(\mathbf{d}^*\mathbf{i}_c + \mathbf{d}\mathbf{i}_c^*) \tag{5}$$

where the superscript '*' denotes complex conjugate. The capacitor current in terms of the three-phase switching functions and filter currents can also be obtained as

$$i_{cap} = \frac{1}{2}\left(d_a i_{ca} + d_b i_{cb} + d_c i_{cc}\right) \tag{6}$$

where (d_a, d_b, d_c) represent the bipolar switching functions of the converter legs.

III. FIR Predictor-Based Control

The current control strategy for the filter is based on the method presented in [37]. In (1) let the reference for the filter current be obtained by subtracting the measured load current space vector from the reference source current space vector as

$$\mathbf{i}_c^{\otimes} = \mathbf{i}_s^{\otimes} - \mathbf{i}_L \tag{7}$$

where '$^{\otimes}$' denotes a reference value. In order to achieve a unity power factor operation, the reference for the current $\mathbf{i}_s^{\otimes}$ should be in the form of (4) and therefore, is chosen as follows

$$\mathbf{i}_s^{\otimes} = I_{sm}(t)\, e^{j\omega t} \tag{8}$$

where $I_{sm}(t)$ is the time-varying reference amplitude determined by a proportional-integral (PI) voltage regulator as

$$I_{sm}(t) = K_p \Delta v_c + K_i \int \Delta v_c \, dt \tag{9}$$

In (9), Δv_c is the error between the actual capacitor voltage and its reference defined as $\Delta v_c = v_c - V_c^{\otimes}$ where $V_c^{\otimes}$ is the reference for the capacitor voltage. Now let the switching function space vector be determined by

$$\mathbf{d} = \frac{2}{v_c}\left[\mathbf{e} - L\frac{d\mathbf{i}_c^{\otimes}}{dt} - R_l \mathbf{i}_c^{\otimes} + K_c \Delta \mathbf{i}_c\right] \tag{10}$$

where $\Delta \mathbf{i}_c = \mathbf{i}_c - \mathbf{i}_c^{\otimes}$ is the error between the actual filter current and its reference. The gain K_c is included to control the time constant with which the current error decays to zero (see (11)). Substitution of (10) into (1) yields

$$L\frac{d\Delta \mathbf{i}_c}{dt} + (R_l + K_c)\Delta \mathbf{i}_c = 0 \tag{11}$$

It is evident from (11) that the current error converges to zero at a rate determined by the time-constant $\tau = L/(R_l + K_c)$. After the filter current error converges to zero, the filter current is forced to track its reference under all circumstances provided that the switching function space vector in (10) is not saturated. Note that the control in (10) leads to the decoupling of the current control loop from that of the voltage control. Equations (9) and (10) are the control equations of the proposed active filter strategy.

For a microcontroller-based implementation in discrete-time, the control equations must be discretized. At $t = kT_s$, the switching function space vector becomes

$$\mathbf{d}(k) = \frac{2}{v_c(k)}\left[\mathbf{e}(k) - L_e\left(\frac{d\mathbf{i}_c^{\otimes}}{dt}\right)_{(k)} - R_l \mathbf{i}_c^{\otimes}(k) + K_c \Delta \mathbf{i}_c(k)\right] \tag{12}$$

where

$$\left(\frac{d\mathbf{i}_c^{\otimes}}{dt}\right)_{(k)} \equiv \frac{1}{T_s}\left[\mathbf{i}_c^{\otimes}(k) - \mathbf{i}_c^{\otimes}(k-1)\right]$$

is the backward difference approximation for the reference current derivative. Note that in (12) the estimated value of the filter inductance L_e is used, as it may differ from the actual value in the system (the estimated and actual values of the inductor resistance are assumed to be equal, since the gain K_c is much larger than the resistance). However, the switching function space vector computation defined in (12) requires a multiplication by 2 and a division by $v_c(k)$. Therefore, in order to avoid this, different from [37], a new control variable may be defined as follows

$$\begin{aligned}\mathbf{u}(k) &\equiv \frac{1}{2}\mathbf{d}(k)v_c(k) = \\ &= \mathbf{e}(k) - L_e\left(\frac{d\mathbf{i}_c^{\otimes}}{dt}\right)_{(k)} - R_l \mathbf{i}_c^{\otimes}(k) + K_c \Delta \mathbf{i}_c(k)\end{aligned} \tag{13}$$

In a real-time implementation, calculation of the control variable will start at the sampling time t_k after the acquisition of all the variables. The time required for the analog-to-digital (A/D) conversions of these variables and control calculations is usually a large fraction of the sampling period. Furthermore, the control variable cannot be applied to the converter as soon as its calculation is completed. Doing so would lead to a time delay which would be difficult to compensate for. Instead, the control $\mathbf{u}(k)$ would be applied at the start of the next sampling interval, resulting in a one-sampling-period delay. The effect of this delay has been observed as inability of the controller in following the fast changes in the load current, with the result that THD of grid currents is considerably increased (see Section IV). To avoid this delay, the control $\mathbf{u}(k+1)$ should be calculated in the sampling period starting at t_k, which requires that the values of all the variables at time t_{k+1} must be predicted. This could be done by employing the model of the system to predict the controlled variables, and by using, for instance, polynomial prediction for the reference variables. Such a scheme, however, has the disadvantages that the predictions of the controlled variables would depend on the parameters of the system, and that the computational complexity of the control algorithm would be increased. These can be avoided if only the resultant control variable is predicted in such a way that the capability to compensate for the significant low-order harmonics is not compromised. The value of $\mathbf{u}(k)$ at time t_k can be predicted by a FIR predictor as

$$\hat{\mathbf{u}}(k) = \sum_{n=1}^{N} b_n \mathbf{u}(k-n) \tag{14}$$

The design of the FIR predictor is described in the next section. As explained above, this approach is different from the model-based predictive control described in the literature [30]. An advantage of the proposed approach is that dependence of the predictions on the system parameters is significantly reduced. The only variable dependent on the parameters is the control given by (13).

Analysis of the current control loop in the steady state may reveal the effectiveness and possible shortcomings of this approach. The closed-loop equations of the filter may be obtained by first discretizing the filter equations in (1). Using forward difference approximations for the derivatives in (1) and (13), we obtain

$$\mathbf{i}_c(k+1) = \mathbf{i}_c(k) + \frac{T_s}{L}\left[\mathbf{e}(k) - \hat{\mathbf{u}}(k) - R_l \mathbf{i}_c(k)\right] \tag{15}$$

Substitution of (13) and (14) in (15) gives after simplification

$$\Delta\mathbf{i}_c(k+1)-\alpha_0\Delta\mathbf{i}_c(k)+\frac{K_cT_s}{L}\sum_{n=1}^{N}b_n\Delta\mathbf{i}_c(k-n)=\frac{T_s}{L}\Delta\hat{\mathbf{e}}(k)$$
$$+\alpha_0\mathbf{i}_c^{\otimes}(k)-\mathbf{i}_c^{\otimes}(k+1)+\alpha_1\sum_{n=1}^{N}b_n\mathbf{i}_c^{\otimes}(k-n)-\alpha_2\sum_{n=1}^{N}b_n\mathbf{i}_c^{\otimes}(k-n-1) \quad (16)$$

where

$$\alpha_0=\left(1-\frac{R_lT_s}{L}\right)\quad,\quad \alpha_1=\frac{L_e}{L}+\frac{R_lT_s}{L}\quad,\quad \alpha_2=\frac{L_e}{L}$$

and the prediction error of $\mathbf{e}(k)$ is defined as

$$\Delta\hat{\mathbf{e}}(k)=\mathbf{e}(k)-\sum_{n=1}^{N}b_n\mathbf{e}(k-n)$$

The error transfer function relating the current error to the filter reference current is obtained as

$$H_e(z)=\frac{\Delta\mathbf{i}_c(z)}{\mathbf{i}_c^{\otimes}(z)}=\frac{\alpha_0-z+(\alpha_1-\alpha_2z^{-1})\sum_{n=1}^{N}b_nz^{-n}}{z-\alpha_0+\frac{K_cT_s}{L}\sum_{n=1}^{N}b_nz^{-n}} \quad (17)$$

Ideally, the predictor coefficients should be chosen to minimize a cost function defined in terms of the frequency response of (17). However, such a cost would be a highly nonlinear function of the coefficients, rendering the optimization procedure difficult. An insight into the frequency response of the error transfer function can be gained by neglecting the error of prediction in (14) and the error in the inductance (L_e=L). This corresponds to replacing the summations in (17) by unity, which gives after simplification

$$H_e(z)=\frac{\Delta\mathbf{i}_c(z)}{\mathbf{i}_c^{\otimes}(z)}=\frac{2-z-z^{-1}}{z-p}\quad,\quad p=1-\frac{T_s}{L}(R_l+K_c) \quad (18)$$

Fig. 2 shows the magnitude response of (18) plotted for the parameter values used in the experimental system (for K_c = 5). It can be observed that even with ideal prediction, higher order harmonics tend to be amplified (harmonics at frequencies greater than 0.9871 rad are amplified). This is a consequence of discrete-time control, and the only remedy is to make the sampling frequency as high as possible. It should be noted that, even with model-based prediction, this behavior would arise as a result of the prediction of reference variables, which are not related with the system model (since they involve the unknown load current).

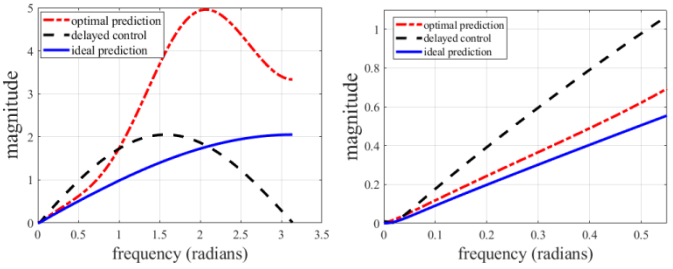

(a) (b)

Fig. 2. (a) Magnitude responses of $H_e(z)$ with ideal and optimal predictors, and with delayed control, (b) Magnified version showing low frequency range.

The poles of the current control loop are given by the zeros of the denominator polynomial in (17), which is independent of the estimated inductance. Hence, stability of the current loop depends only on the gain K_c and the predictor coefficients. With ideal prediction the single pole is given by p in (18). The poles of (17) using the optimal predictor coefficients (obtained in the next section) are calculated as

$$p_1=0.938,\ p_2=0.282,\ p_3=-0.085,\ p_{4,5}=-0.068\pm j0.360$$

It should be noted that in (13), a sudden change in the filter current reference may give rise to saturation of the switching function as a result of the derivative. However, this saturation will last at most a couple of sampling periods, in which the state variables are determined by an uncontrolled operation. At the end of this interval, the system will resume linear unsaturated operation from a new operating point that the system states are taken to by the saturated operation. Therefore, the system's stability will not be affected in general.

A. Design of the FIR Predictor

The transfer function relating the prediction error to the signal to be predicted may be obtained from (14) as

$$H_{pe}(z)=1-\sum_{n=1}^{N}b_nz^{-n} \quad (19)$$

Given a fixed length N of the filter, the cost function to be minimized is

$$J=\sum_{h=1}^{h_{\max}}Q(m_h\omega_0)\left|H_{pe}(m_h\omega_0)\right|^2 \quad (20)$$

which is a weighted sum of the squared-error magnitudes at the harmonic frequencies. In (20), m_h are the harmonic orders and $h_{\max}$ is the index corresponding to the maximum frequency harmonic in the signal. Q is a weight function which is included to enable the shaping of the frequency response of the error transfer function. For instance, lower order harmonics having larger magnitudes may be assigned higher weights. The prediction error transfer function in the frequency domain can be written as

$$H_{pe}(e^{j\omega})=1-e^{j\omega}\mathbf{b}^T\mathbf{s}(\omega) \quad (21)$$

where $\mathbf{s}(\omega)=[1\quad e^{-j\omega}\quad\cdots\quad e^{-j(N-1)\omega}]^T$. Substituting (21) in (20) and equating the gradient with respect to the vector $\mathbf{b}$ to zero gives the solution for the unknown vector of coefficients as

$$\mathbf{b}=\left[\sum_{h=1}^{h_{\max}}Q(\omega_h)\mathbf{F}(\omega_h)\right]^{-1}\left[\sum_{h=1}^{h_{\max}}Q(\omega_h)\mathbf{c}(\omega_h)\right] \quad (22)$$

where

$$\mathbf{F}(\omega_h)=\mathrm{Re}\left\{\mathbf{s}(\omega_h)\mathbf{s}^H(\omega_h)\right\}=\mathrm{Toepl}\left\{1,\cos(\omega_h),\cdots,\cos((N-1)\omega_h)\right\} \quad (23)$$

$$\mathbf{c}(\omega_h)=\left[\cos(\omega_h)\quad\cos(2\omega_h)\quad\cdots\quad\cos(N\omega_h)\right]^T \quad (24)$$

In (23) Toepl refers to a Toeplitz matrix with the first row given by the arguments. Corresponding to the harmonic orders m_h = 1, 5, 7, 11, 13,…, $m_{h\max}$, and using appropriately chosen weights, the predictor coefficients are calculated for N = 4 as $\mathbf{b}=[2.33\quad -1.7915\quad 0.4085\quad 0.0496]^T$. The weights ($Q(\omega_h)$) are chosen in order to match as closely as possible the frequency response of the predictor to that of the ideal one.

Starting with a set of suitable values, the weights are fine-tuned in an iterative manner until a satisfactory response is obtained. The qualitative objectives aimed at in this procedure are that the low-order harmonics are accurately predicted, while the higher order ones are not excessively amplified (Inherently, these two objectives are opposing, and with a finite-length predictor a compromise needs to be made between the two). Fig. 2 shows the magnitude response of the current error with these predictor coefficients. It is observed that with the optimized filter, the magnitude response closely follows that of ideal prediction at low frequencies, but deviates from it at higher frequencies. This deviation is the result of imposing much larger weights to the low-order harmonics. The large magnitude in the high frequency range is not expected to give rise to adverse effects, because harmonics in the load current at these frequencies are negligibly small. It should be noted that, due to limitations on the number of arithmetic operations that can be executed within one sampling period, the length of the FIR predictor has been kept small at $N = 4$. Larger values of N would result in a better magnitude response. Fig. 2 also shows the response with delayed control (one sampling period delay), where the error in the low-order harmonics is much larger than that with optimal prediction.

B. Selection of K_c

The dependence of the current error on the gain K_c is investigated to determine the most appropriate value. In order to achieve this, the theoretical rms current error defined in (25) is calculated using (17) for a range of K_c values.

$$I_{e,rms} = \left(\sum_{k=1,5,7,\ldots} \left| \Delta i_c(e^{jk\omega_s}) \right|^2 \right)^{\frac{1}{2}} = \left(\sum_{k=1,5,7,\ldots} \left| H_e(e^{jk\omega_s}) \right|^2 I_{ck}^2 \right)^{\frac{1}{2}} \tag{25}$$

This calculation assumes that the load current is a quasi-square-wave, with harmonic amplitudes I_{ck} relative to the fundamental, and with a displacement factor of 0.8. Fig. 3(a) indicates that the current error is not very sensitive to K_c. However, selection of the gain K_c is a matter of conflicting criteria. On the one hand, K_c has a slight effect on the steady state current error. As indicated in Fig. 3(a), either a very small value or a very large value for K_c should be chosen in order to minimize the current error. On the other hand, a very small value of K_c would lead to a slow response of the filter current (see (11)), and a large value may give rise to saturation of the switching function when the current error is large. Therefore, selection of K_c should be based on considerations such as time constant of the current loop, and the linearity of the PWM process. It is worth mentioning that the rms current error values in Fig. 3(a) are representative of the actual THD values of the grid current.

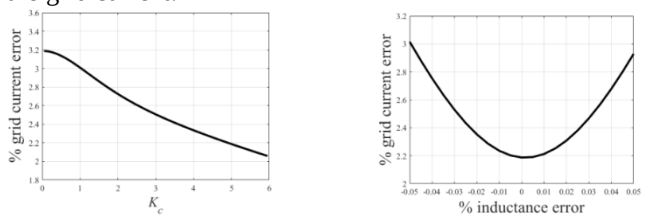

(a) (b)

Fig. 3. (a) Dependence of current error on K_c, (b) Theoretical variation of grid current rms error with error in inductance (K_c=5).

C. Robustness

Investigation of the sensitivity of the current error to uncertainties in the filter parameters is important to ensure that the predictor does not deviate much from optimal. Fig. 3(b) shows the current error as a function of the relative error in the inductance value defined as $(L_e - L)/L$, where L_e and L are the estimated and actual values respectively. Here the relative error is varied in a range corresponding to ±5% change in the estimated inductance value. It can be noticed that the current error for negative values of inductance error is less than that for the nominal inductance value over a large part of the error range. For positive values of inductance error the current error increases steadily as inductance error increases. This increase, however, may be considered within acceptable limits.

Robustness of the closed-loop system regarding stability in the presence of parameter uncertainties may also be inferred from the transfer function in (17), where poles of the system are given by the zeros of the denominator polynomial. Evidently, however, closed-loop poles are not affected by an uncertainty in the filter inductance, since the denominator does not involve the estimated inductance value.

D. Stability Analysis of the Voltage Control Loop

The choice of the PI controller gains K_p and K_i should be based on a small-signal analysis of the closed-loop system. The resistance R_l may be neglected to simplify the analysis. Inclusion of R_l gives rise to transcendental equations and makes it impossible to obtain a closed-form solution for the steady state operating point. In the following analysis, a sinusoidal load current is assumed. Defining the perturbation variables

$$x_1 = I_{sm} - I_{smo} \quad , \quad x_2 = v_c - V_c^{\otimes} \tag{26}$$

where I_{smo} is the steady-state value of the source current amplitude and is equal to $I_{Lm}\cdot\cos(\phi)$ for unity power factor operation, the filter reference current then becomes

$$\mathbf{i}_c^{\otimes} = \left[(I_{smo} + x_1) - I_{Lm} e^{j\varphi} \right] e^{j\omega t} = \left(x_1 - jI_{Lm}\sin(\varphi) \right) e^{j\omega t} \tag{27}$$

It may be safely assumed that the dynamics of the current control loop are much faster than those of the voltage loop. Hence, the filter current error can be assumed to be negligible as far as the voltage control loop is concerned. In this case, the switching function becomes

$$\mathbf{d}(k) = \frac{2}{v_c(k)} \left[\mathbf{e}(k) - \frac{L}{T_s} \left(\mathbf{i}_c^{\otimes}(k) - \mathbf{i}_c^{\otimes}(k-1) \right) \right] \tag{28}$$

Then, using (27) and (28), the right-hand-side of (5) with $\mathbf{i}_c = \mathbf{i}_c^{\otimes}$ can be evaluated at time $t = kT_s$ to give

$$\begin{aligned} \frac{3}{8}\left[\mathbf{d}^* \mathbf{i}_c^{\otimes} + \mathbf{d}(\mathbf{i}_c^{\otimes})^* \right] = \frac{3}{2v_c(k)} \Bigg[& E_m x_1(k) - \frac{L}{T_s} x_1(k)\left(x_1(k) - c_0 x_1(k-1) \right) \\ & - \frac{L}{T_s} I_{Lm}^2 \sin^2\varphi (1 - c_0) - \frac{L}{T_s} I_{Lm} \sin\varphi \left(x_1(k) - x_1(k-1) \right) s_0 \Bigg] \end{aligned} \tag{29}$$

where $c_0 = \cos(\omega_0)$, $s_0 = \sin(\omega_0)$ and $\omega_0 = 2\pi f / f_s$ is the discrete-time fundamental frequency. The PI controller in (9) can be discretized as

$$I_{sm}(k) = I_{sm}(k-1) + (K_p + K_i T_s)\Delta v_c(k) - K_p \Delta v_c(k-1) \tag{30}$$

which is the equation used in the experimental system. New

state variables must be defined so that the dynamical equations can be written in state-space form, as follows

$\xi_1(k)=x_1(k-1),\ \xi_2(k)=x_1(k),\ \xi_3(k)=x_2(k-1),\ \xi_4(k)=x_2(k)$

Based on the assumption that $f<<f_s$ the approximations $c_0\cong 1,\ s_0\cong 0$ can be made. Then, the linearized discrete-time dynamical equations of the closed system are obtained as

$$\begin{aligned}\xi_1(k+1)&=\xi_2(k)\\ \xi_2(k+1)&=(1+\beta K_1)\xi_2(k)+(K_1+K_2)\xi_4(k)\\ \xi_3(k+1)&=\xi_4(k)\\ \xi_4(k+1)&=\beta\xi_2(k)+\xi_4(k)\end{aligned}\tag{31}$$

where

$$\beta=\frac{3T_sE_m}{2CV_{cr}},\quad K_1=K_p+K_iT_s,\qquad K_2=-K_p$$

The characteristic equation of the system (31) is the following

$$D(z)=z^2\left[z^2-(2+\beta K_1)z+1-\beta K_2\right]\tag{32}$$

Stability of the system requires that the roots of (32) are on the unit disc, which yields the following ranges for the gains,

$$-\frac{2}{\beta}<K_p<0,\qquad K_iT_s>-2K_p-\frac{4}{\beta}\tag{33}$$

The poles of the voltage control loop can be placed at desired locations by an appropriate choice of the gains subject to the constraints (32).

E.Comparison with Other Predictive Control Strategies

The existing predictive control strategies are compared with the proposed control strategy. The comparison is based on quantitative analysis in terms of dc-bus voltage control, reference filter current estimation method, sampling period delay compensation method, robustness to parameter variations, switching frequency, weighting factor selection method, cost function optimization as shown in Table I. It can be seen that the proposed control outperforms better than the other methods in terms of reference filter current estimation, sampling period delay compensation, robustness, weighting factor selection, and cost function optimization. Furthermore, the method in [28] makes use of mean value of current during sampling. It is almost impossible to acquire accurate mean value which implies that the value of current in the next period will be inaccurate. In [30], an extrapolation based harmonic command current prediction method is adopted. With a higher order of the polynomial, the current prediction of the method can be more accurate, but it will increase the computation burden which also may increase the calculation time when it is accomplished in a processor with low speed of calculation. The problem is complicated by the fact that the harmonic currents which need to be cancelled have to be identified. The identification algorithm employed will itself have an influence on the dynamic behavior of the system. The method in [32] has one-step delay which degrades the performance. According to [33], in order to compensate this one step delay in digital control, the cost function considering the tracking error at $(k+2)^{th}$ instant should be evaluated. The method in [36] uses three PI controllers for each phase.

F. Extension of FIR Predictor-Based Control to LCL Filter Interfaced Shunt APF

The proposed FIR predictor-based control can easily be adopted to LCL-filter interfaced shunt APF system shown in Fig. 4. The equations in the stationary reference frame can be written in the vector form as follows

$$R_{l1}\mathbf{i}_{c1}+L_1\frac{d\mathbf{i}_{c1}}{dt}=\mathbf{e}-\mathbf{v}_{Cf}\tag{34}$$

$$R_{l2}\mathbf{i}_{c2}+L_2\frac{d\mathbf{i}_{c2}}{dt}=\mathbf{v}_{Cf}-\tfrac{1}{2}\mathbf{d}\,v_c\tag{35}$$

$$C_f\frac{d\mathbf{v}_{\mathbf{Cf}}}{dt}=\mathbf{i}_{c1}-\mathbf{i}_{c2}\tag{36}$$

where $\mathbf{i}_{c1}$ denotes the grid-side current space vector, $\mathbf{i}_{c2}$ denotes the converter-side current space vector, $\mathbf{v}_{Cf}$ denotes the filter capacitor voltage space vector. Solving for the switching function space vector from (35) and adding $K_c\Delta\mathbf{i}_{c2}$ yields

$$\mathbf{d}=\frac{2}{v_c}\left[\mathbf{v}_{Cf}-L_2\frac{d\mathbf{i}_{c2}^{\otimes}}{dt}-R_{l2}\mathbf{i}_{c2}^{\otimes}+K_c\Delta\mathbf{i}_{c2}\right]\tag{37}$$

where $\Delta\mathbf{i}_{c2}=\mathbf{i}_{c2}-\mathbf{i}_{c2}^{\otimes}$, $\mathbf{i}_{c2}^{\otimes}=\mathbf{i}_{c1}^{\otimes}-\mathbf{i}_C$, $\mathbf{i}_{c1}^{\otimes}=\mathbf{i}_s^{\otimes}-\mathbf{i}_L$ and $\mathbf{i}_C$ denotes capacitor current space vector. It should be noted that $\mathbf{i}_s^{\otimes}$ can be obtained as in (8). Hence, the FIR predictor-based control can be adopted to (37). The LCL filter would yield much lower switching frequency distortion in the grid current, however at the expense of increased complexity of the control strategy. It is well-known from research on grid-connected inverters that are coupled to the grid through LCL filters, control design is faced with the problem of resonance of the LCL circuit. The control structure must be designed to provide sufficient damping of the resonance that may arise. In the APF case, the resonance problem is even worse, since the filter current would contain low order harmonics that are highly likely to cause resonance, requiring significantly more suppression of the resonance. Designing a controller which would handle the resonance problem in addition to accomplishing the usual APF function is quite challenging.

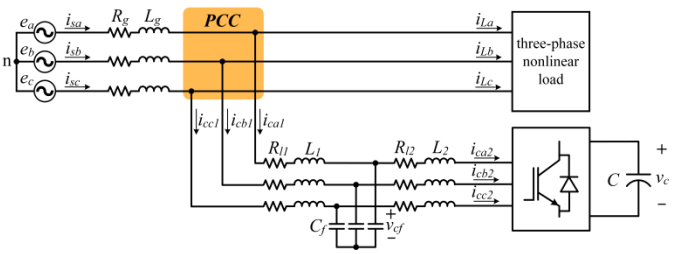

Fig. 4. Three-phase LCL-filter interfaced shunt APF.

TABLE I
COMPARISON OF SEVEN CONTROL METHODS WITH PROPOSED CONTROL METHOD

Category	Dc-bus voltage control	Method of reference filter current estimation	Method of sampling period delay compensation	Robustness study/ Robustness to parameter variations	Switching frequency	Method of weighting factor selection	Cost function optimization
[28]	Achieved with PI	Averaging	None	Sensitive to L	Constant	Does not apply	Does not apply
[30]	Achieved with PI	Repetitive predictor	One-sample-ahead prediction	Closed-loop poles are dependent on L	Space vector method	Heuristic	Does not apply
[32]	Achieved without PI	Kalman filter	None	Sensitive to L	Time-varying	Does not apply	Does not apply
[33]	Achieved with PI	dq-based system (5 multiplications, 2 additions, 1 subtraction)	None	Sensitive to L	Time-varying	None	Online
[34]	Achieved without PI	Instantaneous power theory & HPF	None	Not reported	Time-varying	Heuristic	Online
[35]	Achieved without PI	Prediction & Resonant filter	Prediction	Sensitive to L	Constant	Heuristic	Online
[36]	Achieved with PI	LMS based ADALINE	None	Not reported	Constant	Does not apply	Does not apply
Proposed	Achieved with PI	1 subtraction	FIR prediction	Closed-loop poles are not dependent on L	Constant	Analytical	Offline

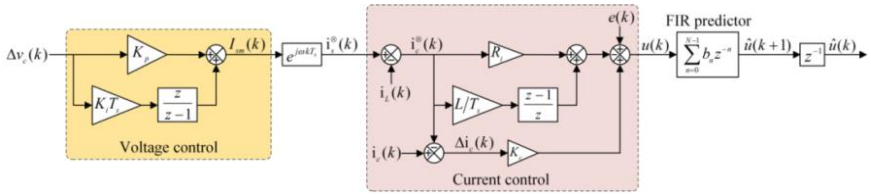

Fig. 5. Block diagram of the proposed predictive control.

IV. SIMULATION AND EXPERIMENTAL RESULTS

The effectiveness of the proposed control strategy is tested by simulations and experimentally on a three-phase shunt APF system. The block diagram of the proposed predictive control is depicted in Fig. 5. The active filter prototype is realized using a Guasch MTL-CBI0060F12IXHF full bridge. An AMREL SPS1000-10-K0E3 source is used for the grid voltage. The control strategy is implemented on a floating-point TMS320F28M36 digital signal processor. The parameters of the system are given in Table II. In the experimental system, a diode bridge rectifier which is connected to PCC by an inductor of 5mH is utilized as nonlinear load.

TABLE II
PARAMETERS OF THE THREE-PHASE APF SYSTEM

Parameter	Value
Grid voltage amplitude, E_m	150V
DC-bus voltage reference, $V_c^{\otimes}$	400V
Converter power, P_c	1500W
Grid line inductance, L_g	0.1mH
Grid line resistance, R_g	0.05Ω
Input filter inductance, L	5mH
Input filter resistance, R_l	0.0493Ω
DC-bus capacitor, C	1000μF
Proportional gain, K_p	-0.01
Integral gain, K_i	-2
Time constant control gain, K_c	5
Grid frequency, f	50Hz
Sampling frequency, f_s	20kHz
Switching frequency, f_{sw}	10kHz

A. Simulation Results

Fig. 6 shows the steady-state simulation results under balanced and sinusoidal grid voltage condition obtained by the proposed control method. It can be seen that the grid currents are almost sinusoidal and in phase with the grid voltages. The THD of grid currents is computed as 3.67%.

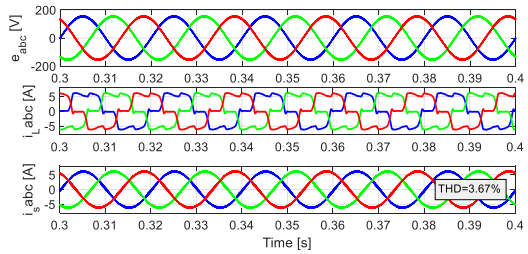

Fig. 6. Steady-state responses of three-phase grid voltages, load currents, and grid currents under balanced and undistorted grid voltages.

Fig. 7 shows the steady-state simulation results under unbalanced grid voltage condition where phase B and phase C voltages are reduced to 90% and 80% of the nominal value. Despite unbalanced grid voltages, the grid currents are still balanced. The THD of grid currents is computed as 3.76%.

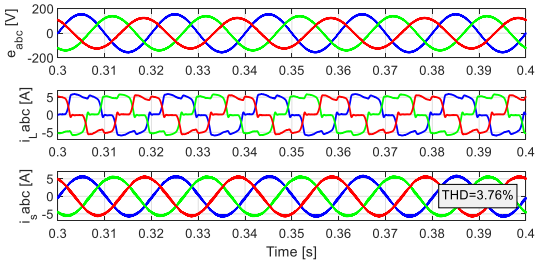

Fig. 7. Steady-state responses of three-phase grid voltages, load currents and grid currents under unbalanced and undistorted grid voltages.

Fig. 8 shows the steady-state simulation results under unbalanced grid voltages where load consumes reactive power. The grid currents are balanced with a THD equal to 3.76%.

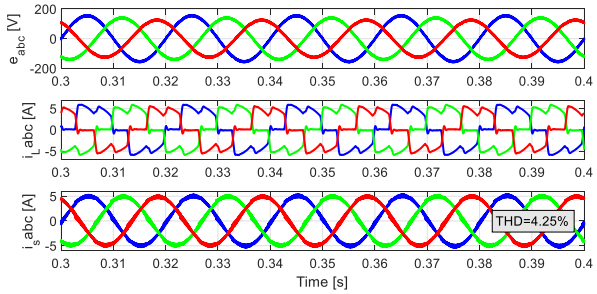

Fig. 8. Steady-state responses of three-phase grid voltages, load currents and grid currents under unbalanced grid voltages where load consumes reactive power.

Fig. 9 shows the steady-state simulation results under distorted grid voltage condition where grid voltages contain 10% 5th harmonics. Despite the distorted grid voltage, the grid currents are almost sinusoidal. The THD of grid currents is computed as 3.71%. Fig. 10 shows the steady-state simulation results under ±5% mismatch in L_e. Clearly, the grid currents under both cases are sinusoidal with THD values computed as 4.04% and 3.64%. As mentioned in Section III-C, the stability of closed-loop system is not affected from the uncertainty in L_e.

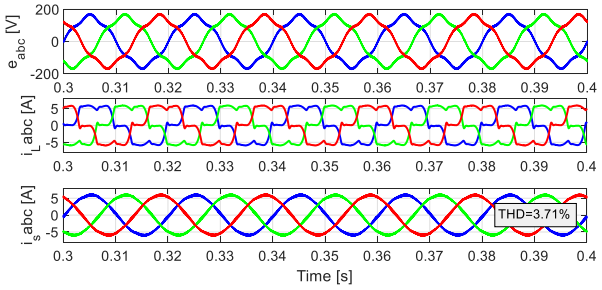

Fig. 9. Steady-state responses of three-phase grid voltages, load currents, and grid currents under distorted grid voltages.

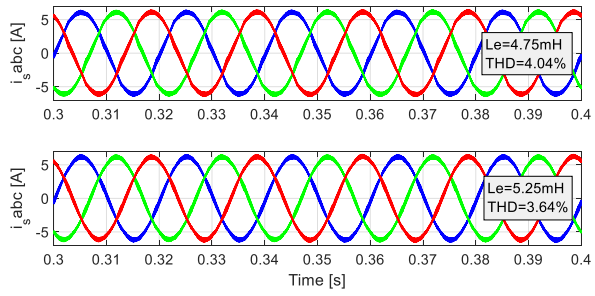

Fig. 10. Steady-state responses of three-phase grid currents under ±5% mismatch in L_e.

Fig. 11 shows the dynamic response of grid voltages, grid currents and dc-bus voltage obtained for a sudden change in the resistive load from 88Ω to 44Ω. It is obvious that the dc-bus voltage exhibits undershoot and settles down at 400V after a few cycles. The grid currents exhibit faster dynamic response than that of dc-bus voltage. It is worth noting that the dynamic response of dc-bus voltage can be faster by increasing K_c provided that the switching function is not saturated as mentioned in Section III-B.

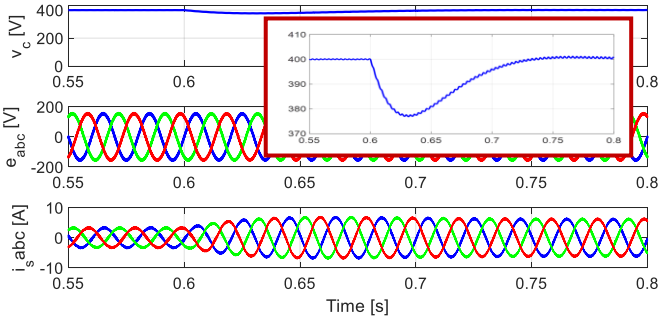

Fig. 11. Dynamic responses of three-phase grid voltages and currents and dc-bus voltage obtained by the proposed control method using FIR predictor.

Fig. 12 shows start-up responses of dc-bus voltage, grid currents, and filter currents. Initially, the system is started without APF where the dc-bus voltage is 270V. In this case, the grid currents are highly distorted since APF does not inject any compensation current ($i_{c,\,abc} = 0$) to PCC and therefore the grid currents are equal to the load currents ($i_{s,\,abc} = i_{L,\,abc}$). When the APF is enabled, the controller acts accordingly to regulate the dc-bus voltage and grid currents. In this case, the compensation currents are not zero anymore. The grid currents are almost sinusoidal with reasonably low distortion. Since APF is enabled, the currents at PCC satisfy $i_{s,\,abc} = i_{L,\,abc} + i_{c,\,abc}$. On the other hand, the dc-bus voltage gradually rises from 270V to 400V.

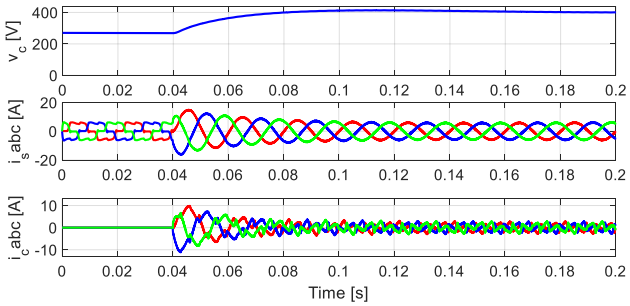

Fig. 12. Startup responses of three-phase grid voltages, grid currents and dc-bus voltage obtained with proposed control method.

B. *Experimental Results*

Fig. 13 shows the steady-state responses of three-phase grid voltages, grid currents and dc-bus voltage obtained without and with FIR predictor under a diode bridge rectifier load. It is worth noting that the results obtained without FIR predictor involve the effect of one-sampling-period delay. In other words, the control **u**(k) in (13) is utilized to control the APF. It can be seen that the grid currents are in phase with the corresponding grid voltages in both cases. Also, in both cases, the dc-bus voltage is regulated at the desired reference value which is 400V. The distortion of grid currents obtained without FIR predictor is discernible in Fig. 13(a).

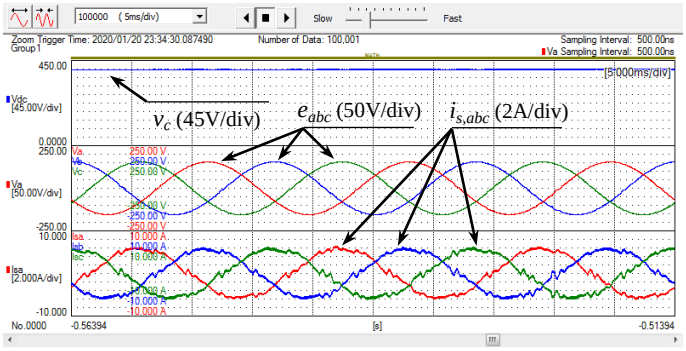

(a)

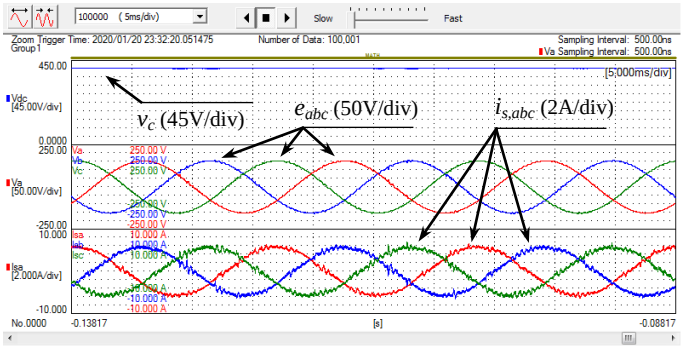

(b)

Fig. 13. Steady-state responses of three-phase grid voltages, grid currents and dc-bus voltage obtained: (a) Without FIR predictor, (b) With FIR predictor.

However, when the FIR predictor is employed, the distortion of the currents is reduced considerably as shown in Fig. 13(b). The measured spectrums of the currents with and without FIR predictor are shown in Fig. 14. The total harmonic distortion (THD) of the grid current is measured to be 2.27% and 5.01% with and without the FIR predictor. These results, when compared with the measured load current THD of 24.05% indicate that the proposed APF operates with high performance.

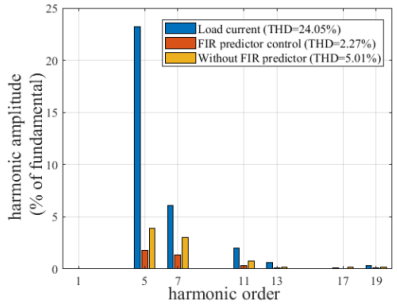

Fig. 14. Measured spectrums of load currents and grid currents (with and without FIR predictor).

Fig. 15 shows the dynamic responses of grid voltages, grid currents and dc-bus voltage obtained without and with FIR predictor for a sudden change in the resistive load from 88Ω to 44Ω. It can be seen that the amplitude of the grid currents is doubled in accordance with the reference amplitude generated by PI regulator. This means that the grid currents track the reference grid currents without and with FIR predictor. Although dc-bus voltage is regulated at 400V, its dynamic response is much slower than that of the grid currents. The main reason of this comes from the fact that the inner current loop is usually much faster than the outer voltage loop. As pointed out before, the distortion in the grid currents obtained without FIR predictor is visible in Fig. 15(a). However, when FIR predictor is used, this distortion is minimized considerably as shown in Fig. 15(b). Experimental results in Fig. 15(b) correspond to the simulation results in Fig. 11. One can see that both results are in good agreement.

Experimental results in Fig. 16 correspond to the simulation results in Fig. 12. It can be seen that both results agree well.

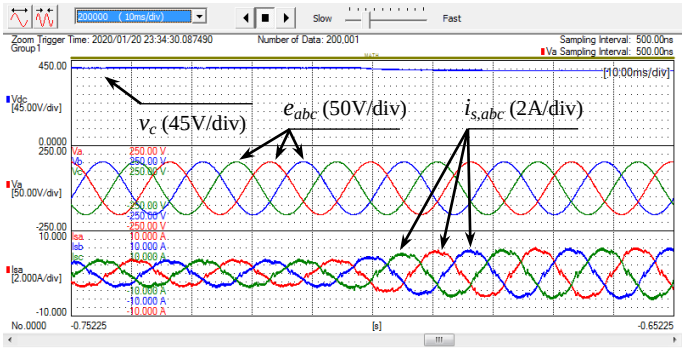

(a)

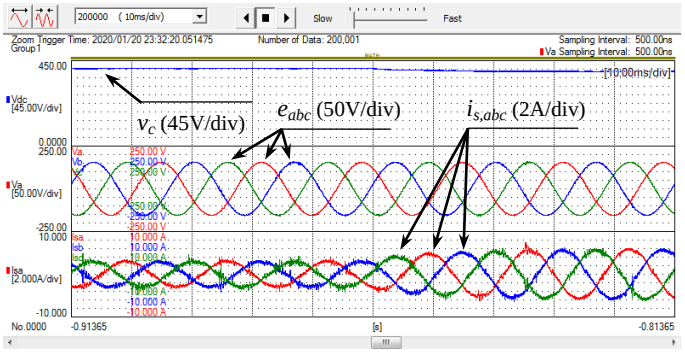

(b)

Fig. 15. Experimental dynamic responses of three-phase grid voltages and currents obtained: (a) Without FIR predictor, (b) With FIR predictor.

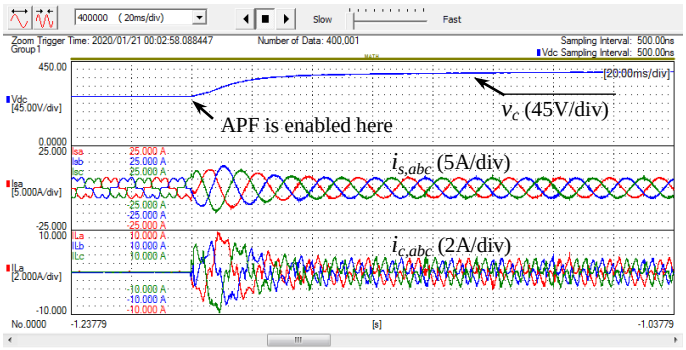

Fig. 16. Experimental startup responses of three-phase grid voltages, grid currents and dc-bus voltage obtained with FIR predictor.

V. Conclusions

A discrete-time FIR-predictor-based control strategy is proposed for three-phase three-wire shunt active power filters. The performance of the control strategy is verified through

simulation and experiments on a laboratory system. It is observed that the proposed control strategy is quite successful in compensating nonlinear load currents. The proposed control strategy has distinct advantages compared to most of the predictive control strategies described in the literature in terms of reference filter current estimation, sampling period delay compensation, robustness against parameter variations, weighting factor selection, and cost function optimization. Unlike existing predictive control methods, the closed-loop poles of the proposed control are not function of the filter inductance which implies that the stability is not affected from the variations in filter inductance. In addition, it is shown that the effect of sampling delay can be compensated by the proposed FIR-predictor.

REFERENCES

[1] IEEE Recommended Practice and Requirements for Harmonic Control in Electrical Power Systems, *IEEE Standard 519-2014*, 2014.

[2] B. Singh, K. Al-Haddad, and A. Chandra, "A review of active filters for power quality improvement," *IEEE Trans. Ind. Electron.*, vol. 46, no. 5, pp. 960–971, May 1999.

[3] S. Rahmani, N. Mendalek, and K. Al-Haddad, "Experimental design of a nonlinear control technique for three-phase shunt active power filter," *IEEE Trans. Ind. Electron.*, vol. 57, no. 10, pp. 3364–3375, Oct. 2010.

[4] R. S. Herrera and P. Salmeron, "Instantaneous reactive power theory: A reference in the nonlinear loads compensation," *IEEE Trans. Ind. Electron.*, vol. 56, no. 6, pp. 2015–2022, Jun. 2009.

[5] M. Cirrincione, M. Pucci, G. Vitale, and A. Miraoui, "Current harmonic compensation by a single-phase shunt active power filter controlled by adaptive neural filtering," *IEEE Trans. Ind. Electron.*, vol. 56, no. 8, pp. 3128–3143, Aug. 2009.

[6] J. M. Kanieski, R. Cardoso, H. Pinheiro, and H. A. Gründling, "Kalman filter-based control system for power quality conditioning devices," *IEEE Trans. Ind. Electron.*, vol. 60, no. 11, pp. 5214–5227, Nov. 2013.

[7] R. Panigrahi, and B. Subudhi, "Performance enhancement of shunt active power filter using a Kalman filter-based H_∞ control strategy," *IEEE Trans. Power Electron.*, vol. 32, no. 4, pp. 2622-2630, April 2017.

[8] S. Jiao, K. R. R. Potti, K. Rajashekara, and S. K. Pramanick, "A novel DROGI-based detection scheme for power quality improvement using four-leg converter under unbalanced loads," *IEEE Trans. Ind. Appl.*, vol 56, no. 1, pp. 815-825, Jan./Feb. 2020.

[9] B. Kedjar, and K. Al-Haddad, "DSP-based implementation of an LQR with integral action for a three-phase three-wire shunt active power filter," *IEEE Trans. Ind. Electron.*, vol. 56, no. 8, pp. 2821–2828, August 2009.

[10] B. N. Singh, B. Singh, A. Chandra and K. Al-Haddad, "Design and digital implementation of active filter with power balance theory," *IEE Proc.- Electric Power Appl.*, vol. 152, no. 5, pp. 1149–1160, September 2005.

[11] O. Vodyakho, and C. C. Mi, "Three-level inverter-based shunt active power filter in three-phase three-wire and four-wire systems," *IEEE Trans. Power Electron.*, vol. 24, no. 5, pp. 1350–1363, May 2009.

[12] R. L. A. Ribeiro, C. C. Azevedo, and R. M. Sousa, "A robust adaptive control strategy of active power filters for power-factor correction, harmonic compensation, and balancing of nonlinear loads," *IEEE Trans. Power Electron.*, vol. 27, no. 2, pp. 718–730, February 2012.

[13] S. R. Choudhury, A. Das, S. Anand, S. Tungare, and Y. Sonawane, "Adaptive shunt filtering control of UPQC for increased nonlinear loads," *IET Power Electronics*, vol. 12, no. 2, pp. 330-336, 2019.

[14] Q. N. Trinh, and H. H. Lee, "An advanced current control strategy for three-phase shunt active power filters," *IEEE Trans. Ind. Electron.*, vol. 60, no. 12, pp. 5400–5410, December 2013.

[15] E. S. Sreeraj, E. K. Prejith, K. Chatterjee, and S. Bandyopadhyay, "An active harmonic filter based on one-cycle control," *IEEE Trans. Ind. Electron.*, vol. 61, no. 8, pp. 3799–3809, August 2014.

[16] N. Mesbahi, A. Ouari, D. O. Abdeslam, T. Djamah, and A. Omeiri, "Direct power control of shunt active filter using high selectivity filter(HSF) under distorted or unbalanced conditions," *Electric Power Syst. Research*, vol. 108, pp. 113–123, 2014.

[17] M. B. Ketzer, and C. B. Jacobina, "Virtual flux sensorless control for shunt active power filters with quasi-resonant compensators," *IEEE Trans. Power Electron.*, vol. 31, no. 7, pp. 4818-4830, July 2016.

[18] H. Zhai, F. Zhuo, C. Zhu, H. Yi, Z. Wang, R. Tao, and T. Wei, "An optimal compensation method of shunt active power filters for system-wide voltage quality improvement," *IEEE Trans. Ind. Electron.*, vol. 67, no. 2, pp.1270-1281, Feb. 2020.

[19] K. Nishida, M. Rukonuzzaman and M. Nakaoka, "Digital control three-phase shunt active power filter with a new harmonic-current-extraction process," *IEE Proc.-Gener. Transm. Distrib.*, vol. 152, no. 4, pp. 529–538, July 2005.

[20] Z. X. Zou, K. Zhou, Z. Wang, and M. Cheng, "Frequency-adaptive fractional-order repetitive control of shunt active power filters," *IEEE Trans. Ind. Electron.*, vol. 62, no. 3, pp. 1659–1668, March 2015.

[21] C. Xie, X. Zhao, M. Savaghebi, L. Meng, J. M. Guerrero, and J. C. Vasquez, "Multirate fractional-order repetitive control of shunt active power filter suitable for microgrid applications," *IEEE Journal of Emerg. and Select. Topics in Power Electron.*, vol. 5, no. 2, pp. 809-819, June 2017.

[22] G. Pandove, and M. Singh, "Robust repetitive control design for a three-phase four wire shunt active power filter," *IEEE Trans. Ind. Inf.*, vol. 15, no. 5, pp. 2810-2818, May 2019.

[23] N. F. A. Rahman, M. A. M. Radzi, A. C. Soh, N. Mariun, and N. A. Rahim, "Adaptive hybrid fuzzy-proportional plus crisp-integral current control algorithm for shunt active power filter operation," *Energies*, vol. 9, pp. 737-754, 2016.

[24] S. Hou, J. Fei, Y. Chu, and C. Chen, "Experimental investigation of adaptive fuzzy global sliding mode control of single-phase shunt active power filters," *IEEE Access*, vol. 7, pp. 64442-64449, 2019.

[25] M. Popescu, A. Bitoleanu and V. Suru, "A DSP-based implementation of the p-q theory in active power filtering under nonideal voltage conditions," *IEEE Trans. Ind. Inf.*, vol. 9, no. 2, pp. 880-889, May 2013.

[26] V. Biagini, P. Zanchetta, M. Odavic, M. Sumner and M. Degano, "Control and modulation of a multilevel active filtering solution for variable-speed constant-frequency more-electric aircraft grids," *IEEE Trans. Ind. Inf.*, vol. 9, no. 2, pp. 600-608, May 2013.

[27] M. Qasim and V. Khadkikar, "Application of artificial neural networks for shunt active power filter control," *IEEE Trans. Ind. Inf.*, vol. 10, no. 3, pp. 1765-1774, Aug. 2014.

[28] S. G. Jeong, and M. H. Woo, "DSP-based active power filter with predictive current control," *IEEE Trans. Ind. Electron.*, vol. 44, no. 3, pp. 329–336, June 1997.

[29] A. Bhattacharya, and C. Chakraborty, "A shunt active power filter with enhanced performance using ANN-based predictive and adaptive controllers," *IEEE Trans. Ind. Electron.*, vol. 58, no. 2, pp. 421–428, February 2011.

[30] M. Odavic, V. Biagini, P. Zanchetta, M. Sumner, and M. Degano, "One-sample-period-ahead predictive current control for high-performance active shunt power filters," *IET Power Electron.*, vol. 4, no. 4, pp. 414–423, 2011.

[31] J. Rodriguez, M. P. Kazmierkowski, J. R. Espinoza, P. Zanchetta, H. Abu-Rub, H. A. Young, and C. A. Rojas, "State of the art of finite control set model predictive control in power electronics," *IEEE Trans. Ind. Inf.*, vol. 9, no. 2, pp. 1003-1016, May 2013.

[32] R. Panigrahi, B. Subudhi, and P. C. Panda, "Model predictive-based shunt active power filter with a new reference current estimation strategy," *IET Power Electron.*, vol. 8, no. 2, pp. 221–233, 2015.

[33] P. Acuna, L. Moran, M. Rivera, R. Aguilera, R. Burgos, and V. G. Agelidis, "A single-objective predictive control method for a multivariable single-phase three-level NPC converter-based active power filter," *IEEE Trans. Ind. Electron.*, vol. 62, no. 7, pp. 4598-4607, July 2015.

[34] K. Antoniewicz, M. Jasinski, M. P. Kazmierkowski, and M. Malinowski, "Model predictive control for three-level four-leg flying capacitor converter operating as shunt active power filter," *IEEE Trans. Ind. Electron.*, vol. 63, no. 8, pp.5255-5262, August 2016.

[35] L. Tarisciotti, A. Formentini, A. Gaeta, M. Degano, P. Zanchetta, R. Rabbeni, and M. Pucci, "Model predictive control for shunt active filters with fixed switching frequency," *IEEE Trans. Ind. Appl.*, vol. 53, no. 1, pp. 296-304, Jan./Feb. 2017.

[36] S. Sharma, V. Verma, and R. K. Behera, "Real-time implementation of shunt active power filter with reduced sensors," *IEEE Trans Ind. Appl.*, vol. 56, no. 2, pp. 1850-1861, March/April 2020.

[37] O. Kukrer and H. Komurcugil, "A new current control strategy for three-phase three wire shunt active power filters," in *Proc. IEEE ISIE*, 2008, Cambridge, UK, pp. 896–901.
[38] F. D. Freijedo, J. Doval-Gandoy, O. Lopez, P. Fernandez-Comesana, and C. Martinez-Penalver, "A signal-processing adaptive algorithm for selective current harmonic cancellation in active power filters," *IEEE Trans. Ind. Electron*., vol. 56, no. 8, pp. 2829-2840, Aug. 2009.
[39] T. Komrska, J. Zak, and Z. Peroutka, "Control strategy of active power filter with adaptive FIR filter-based and DFT-based reference estimation," in Proc. SPEEDAM, 2010, Pisa, Italy, pp. 1524–1529.

Osman Kukrer (M'92-SM'11) received the B.Sc., M.Sc. and Ph.D. degrees from the Middle East Technical University (METU), Ankara, Turkey, in 1979, 1982, and 1987, respectively, all in electrical engineering. He is currently a Professor in the Department of Electrical and Electronic Engineering, Eastern Mediterranean University, Famagusta, North Cyprus, Via Mersin 10, Turkey. His research interests include power electronics, control systems, and signal processing.

Hasan Komurcugil (S'94-M'99-SM'12) received the B.Sc., M.Sc. and Ph.D. degrees from the Eastern Mediterranean University (EMU), Famagusta, North Cyprus, Via Mersin 10, Turkey, in 1989, 1991, and 1998, respectively, all in electrical engineering. He is currently full-time Professor with the Computer Engineering Department, EMU. His research interests include power electronics and innovative control methods for power converters. Prof. Komurcugil is Associate Editor of the IEEE TRANSACTIONS ON INDUSTRIAL ELECTRONICS and IEEE TRANSACTIONS ON INDUSTRIAL INFORMATICS.

Ramon Guzman received the B.S., the M.S. and the Ph.D. degrees in telecommunications engineering from the Technical University of Catalonia, Barcelona, Spain, in 1999, 2004 and 2016, respectively. He is currently an Associate Professor with the Department of Automatic Control at the Technical University of Catalonia. His research interests include nonlinear control and model predictive control for three-phase power converters.

Luis Garcia de Vicuna received the Ingeniero de Telecomunicación and Dr.Ing. degrees from the Technical University of Catalonia, Barcelona, Spain, in 1980 and 1990, respectively, and the Dr.Sci. degree from the Université Paul Sabatier, Toulouse, France, in 1992.
From 1980 to 1982, he was an Engineer with Control Applications Company. He is currently a Full Professor in the Department of Electronic Engineering, Technical University of Catalonia, where he teaches courses on power electronics. His research interests include power electronics modeling, simulation and control, active power filtering, and high-power-factor ac/dc conversion.